Nano Today 59 (2024) 102466

Contents lists available at ScienceDirect

Nano Today

journal homepage: www.elsevier.com/locate/nanotoday

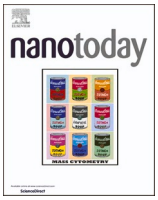

Biotransformation of nanoplastics in human plasma and their permeation through a model *in vitro* blood-brain barrier: An in-depth quantitative analysis

Fazel Abdolahpur Monikh [a,b,c,*,1], Šárka Lehtonen [d,e], Jukka Kekäläinen [b], Isabel Karkossa [f], Seppo Auriola [g], Kristin Schubert [f], Alessandra Zanut [a], Sanni Peltonen [d], Jonna Niskanen [d], Mandar Bandekar [b], Martin von Bergen [f,h,i], Jari T.T. Leskinen [j], Arto Koistinen [j], Sara Bogialli [a], Zhiling Guo [k,l], Jussi V.K. Kukkonen [b], Chunying Chen [m], Iseult Lynch [k,l]

[a] *Department of Chemical Sciences, University of Padua, via Marzolo 1, Padova 35131, Italy*
[b] *Department of Environmental and Biological Sciences, University of Eastern Finland, Joensuu, Kuopio, Finland*
[c] *Institute for Nanomaterials, Advanced Technologies, and Innovation, Technical University of Liberec, Bendlova 1409/7, Liberec 460 01, Czech Republic*
[d] *A.I. Virtanen Institute for Molecular Sciences, University of Eastern Finland, Finland*
[e] *Neuroscience Center, University of Helsinki, Finland*
[f] *Department of Molecular Toxicology, Helmholtz-Centre for Environmental Research GmbH (UFZ), Leipzig, Germany*
[g] *School of Pharmacy, University of Eastern Finland, Kuopio, Finland*
[h] *Institute of Biochemistry, Leipzig University, Leipzig, Germany*
[i] *German Centre for Integrative Biodiversity Research (iDiv) Halle-Jena-Leipzig, Leipzig, Germany*
[j] *SIB Labs, University of Eastern Finland, Kuopio, Finland*
[k] *School of Geography, Earth and Environmental Sciences, University of Birmingham, Edgbaston, Birmingham, United Kingdom*
[l] *Centre for Environmental Research and Justice (CERJ), University of Birmingham, Edgbaston, Birmingham, United Kingdom*
[m] *CAS Key Laboratory for Biomedical Effects of Nanomaterials and Nanosafety, CAS Center for Excellence in Nanoscience, National Center for Nanoscience and Technology of China, China*

ARTICLE INFO

Keywords:
Microplastics
Protein corona
Cytotoxicity
Nanoplastic tracing
Protocol

ABSTRACT

Challenges in characterizing and quantifying nanoplastics within the human body hinder understanding of their transport, biotransformation, and potential for cellular penetration and barrier crossing. By implementing an innovative analytical workflow, including incorporation of gadolinium (Gd) as a tracer into the polymer matrix of nanoplastics, the fate of nanoplastics relative to an in vitro blood-brain barrier (BBB) model is elucidated in the absence or presence of a biomomolecule corona. The nanoplastics were incubated in human plasma for 5 min, 1 h, 6 h, and 24 h, after which the absorbed proteins and lipids (biocorona) were determined. A total of 268 proteins were identified in the biological coronas on polystyrene (PS) and polyvinyl chloride (PVC) nanoplastics, with the initial compositions being broadly similar on both PS and PVC. Both nanoplastics exhibited a strong affinity for phosphatidylcholines (PC) and lysophosphocholines (LPC) from human plasma. The inherent chemical composition of the nanoplastics plays a pivotal role in the corona's evolution over time. Human induced pluripotent stem cell (iPSC)-derived endothelial cells (iECs) and astrocytes were exposed for 2 h to 5 μg L^{-1} of pristine nanoplastics or nanoplastics covered with a biological corona (following incubation in plasma for 6 h). A relatively low concentration of PS and PVC nanoplastics was determined to be present within the cellular layer of the BBB. The number of PVC nanoplastics crossing the BBB was higher than the number of PS nanoplastics. The presence of a biological corona on these particles decreases their uptake and transcytosis. This understanding might further the development of preventive measures or therapeutic strategies to counteract potential nanoplastic-induced neurotoxicity, and provide a foundation for development of *in silico* models to predict the neurotoxic implications of nanoplastics.

* Corresponding author at: Department of Chemical Sciences, University of Padua, via Marzolo 1, Padova 35131, Italy
E-mail addresses: Fazel.Monikh@unipd.it, fazel.monikh@unipd.it (F. Abdolahpur Monikh).
[1] ORCID: Fazel A. Monikh 0000–0001-9500–5303

https://doi.org/10.1016/j.nantod.2024.102466
Received 26 May 2024; Received in revised form 22 July 2024; Accepted 22 August 2024
Available online 31 August 2024

Introduction

Six billion tons' of plastic pollution has been identified in diverse environments, from the deep sea to mountainous areas. Depending on the type of plastic and environmental conditions such as ultraviolet radiation, thermal exposure, and oxidation reactions, these plastic wastes break down into smaller fragments, defined as secondary microplastics, or nanoplastics when the size < 1 μm[1,2]. There is no universally accepted definition for nanoplastics, with some researchers using a size cutoff of 100 nm and others using 1000 nm [3]. Nanoplastics have also been intentionally added to some commercial products, like cosmetics, personal care products, and cleaning agents [4]' [5], although in the EU, the European Commission Regulation (EU) 2023/2055 has banned the intentional addition of microplastics with a phase-in period of 5–8 years [3]. Considering the wide range of plastic applications and thus sources of release to the environment, it's common for individuals to encounter and ingest various types of nanoplastics such as PS, polyethylene (PE), PVC, and polyester via air, water, and food [6]. In human feces, over 95.8 % of samples tested positive for microplastics, with concentrations reaching up to 138.9 items per gram, including fragments, films, and fibers [7]. Several *in vitro* and *in vivo* studies have already indicated the potential adverse effects of inhaled or ingested nanoplastics, including oxidative stress, cellular damage, inflammation, DNA damage, and neurotoxicity [8,9]. However, our understanding of the fate of nanoplastics (i.e., toxicokinetics) within the human body is currently very limited.

Upon first contact with biofluids or the environment, exogenous particles, including nanoplastics, invariably attract a variety of organic molecules from the environment such as volatile organic compounds (VOCs) and/or biomolecules such as metabolites and proteins [10–12]. This adsorption process of biomolecules results in the creation of a 'biological corona' [13,14], a phenomenon attributed to the high free surface energy of these particles and the tendency of biomolecules to adhere to surfaces [15–17]. Consistent with other nanoparticles, previous research has confirmed the immediate formation of a biological corona on nanoplastics as soon as they enter an organism's body [18] as well as the evolution of this corona as nanoplastics move up the food chain [19]. The biological corona determines the particles' biological identity, thereby influencing various aspects of their fate within the body, including toxicokinetics, biodistribution, cellular uptake, and intracellular trafficking [20]. Extensive investigation of the coronas of nanomaterials, including nanoscale PS, has demonstrated that the composition of the biological corona is influenced by the physicochemical properties of the particles (e.g., size, aspect ratio [21], and chemical composition [22]) and the characteristics of the surrounding biofluids. Furthermore, the biological corona's formation is dynamic, undergoing evolution over time as initial adsorption of the most abundant biomolecules occurs which are gradually supplanted by biomolecules with lower abundance but higher affinity [23,24], and biomolecule-biomolecule interactions are typically also involved in recruitment of the evolved corona [25].

The presence of long-lived biomolecules within the biological corona can have significant implications: they may initiate opsonization, thereby facilitating the phagocytic elimination of the particles, or alternatively, dysopsonising proteins extend the particles' circulation duration within the bloodstream. This prolonged presence enhances the potential for these particles to permeate various organs and tissues [23, 26]. Currently, our understanding of the formation and evolution of the biological corona, encompassing proteins and metabolites, on the surface of nanoplastics remains limited, especially in terms of understanding whether primary versus secondary nanoplastics induce different biological coronas due to their different methods of generation, and/or the influence of other incidental co-pollutants such as VOCs. Moreover, the impact of the physicochemical properties of nanoplastics, such as their chemical composition, on the formation and the overall composition of the biological corona has not been systematically investigated.

In humans, the blood-brain barrier (BBB) consists of a tightly packed layer of endothelial cells that separate the blood components from the cerebrospinal fluid, thus preventing most foreign substances from entering the brain [27]. It was recently reported that metallic nanoparticles, such as Ag and ZnO, may penetrate the BBB (ZnO exhibited the highest transport percentage, with 10.5 and 13.4 % of the applied dose translocated at 1 and 2.5 mg/L exposure concentrations, respectively), inducing damage to cell membranes in the brain [28], and affecting cholinergic neurotransmission [29]. Certain metallic nanoparticles have the potential to undergo dissolution within the cellular lysosomal environment, converting them into their ionic forms [30,31]. After dissolution, these ionic forms might utilize pathways meant for soluble chemicals, thereby integrating into the body's regulatory and excretory systems leading to their clearance [32]. This process potentially reduces their accumulation within biological systems. Nanoplastics, which are not easily biodegradable, may pose a risk of accumulating in the brain, as depending on their size, shape, and composition, they appear to have the ability to reach the brain within a few hours after ingestion or inhalation [19,33]. Although some studies have reported that PS nanoplastics might pass through the BBB [34,35], there is still limited knowledge regarding the quantity of nanoplastics that can traverse the BBB. Additionally, how the nanoplastic composition (PVC, PE, PS etc.), and the presence of a protein corona might influence this process remains largely unexplored. This knowledge gap is primarily attributed to the analytical challenges in tracking and quantifying such small polymeric particles at the cellular level in real-time and on a numerical basis [34]. These difficulties arise from the fact that the chemical compositions of nanoplastics bear a close resemblance to that of biogenic polymers, such as proteins, lipids, polysaccharides, and celluloses, which poses a significant analytical challenge in differentiating them. Some progress has been made in tracking nanoplastics in complex matrices using proxies, such as stable isotope or radio-labeling techniques. Recently, labeled or tagged nanoplastics including metal-labeled plastics have been investigated in various model environmental systems at bench-top or pilot-scale [36]. Additionally, microplastics can potentially be identified using techniques like Py-GC-MS and characterized in terms of different physicochemical properties. Nevertheless, this technique faces challenges in tracking nanoplastics in biological samples [37].

To overcome these analytical limitations, our study utilized Gadolinium (Gd) as a tracer by embedding it within nanoplastics. Recently, a few studies have emerged where metals or metallic nanoparticles were embedded in nanoplastics to facilitate tracking of PS nanoplastics in environmental samples [36,38-40]. However, apart from our previous study [19], no research has embedded Gd in nanoplastics other than PS, such as PVC, and tracked the particles in the presence of enzymes and proteins, which could potentially biotransform the particles and lead to metal release. Gd is a rare element in biological systems, and thus its incorporation at low concentrations into nanoplastics serves as a distinct marker, facilitating the detection and quantification of nanoplastics within complex matrices of cells and tissues [19]. Moreover, the presence of Gd enables the use of a range of established analytical methods including single-particle inductively coupled plasma mass spectrometry (spICP-MS) and scanning electron microscopy (SEM) coupled with energy-dispersive spectroscopy (EDS) [19]. Due to the low contrast between polymeric particles and biological background, the application of transmission electron microscopy (TEM) is challenging [41]. However, by incorporating Gd into nanoplastics, TEM can be effectively utilized, and sample preparation protocols including cell fixation and sectioning are used to enhance the distinction between the nanoplastics and the biological background in TEM imaging.

The primary objective of this study is to utilize Gd-entrapped nanoplastics and advanced nano-analytical protocols to analyze the specific metabolites and proteins forming the biological corona acquired by PS and PVC nanoplastics in human plasma, and their subsequent passage through, the cells of an *in vitro* BBB. Additionally, we quantify the

number of nanoplastics that are capable of entering and trasncytosing the BBB in the presence and absence of the biological corona, . This approach will allow for a detailed understanding of how different nanoplastic compositions affect BBB permeability. The importance of this work lies in several key areas: a) by analyzing the specific metabolites and proteins forming the initial biological corona, it is possible to gain insights into how nanoplastics interact with biological systems at the molecular level and assess how the biological corona evolves as nanoplastics move through cellular barriers will help to elucidate the dynamic processes involved in nanoplastic-cell interactions, b) quantifying the number of nanoplastics that can transcytose the BBB in the presence or absence of the biomolecule corona provides crucial data on the potential risks of nanoplastic exposure to brain health. This will improve our understanding of how nanoplastics might be modified by biological systems, affecting their transportation, behavior and toxicity; and c) employing advanced nano-analytical protocols to nanoplastics research will push the boundaries of current methodologies, providing more precise and reliable data.

Results and discussion

Physicochemical properties of the nanoplastics

The pristine PS and PVC nanoplastics were comprehensively characterized utilizing dynamic light scattering (DLS), SEM-EDS, spICP-MS, and zeta potential (ζ) measurements, as detailed in Table 1 with the approaches described in the Supporting Information, Section 1. The nominal particle diameter for PS and PVC are 250 nm, with polydispersity indices (PDI) of 0.1 and 0.2, respectively. The hydrodynamic diameters, as determined by DLS, and the diameters measured by TEM – based on the average of 100 particles for each type of nanoplastic – were consistent with the nominal sizes, indicating a homogeneous size distribution. Raman spectroscopy was employed to determine the polymer compositions of the nanoplastics, as detailed in the Supporting Information (Section 1). Accordingly, aggregations of the particles were prepared on microscope slides to facilitate Raman measurements. The hydrophobicity of the particles was assessed by measuring their contact angles with water, following previously reported methodologies[39]. The PS particles, exhibiting a contact angle of 80 ± 2 degrees, were found to be more hydrophobic compared to the PVC particles, which had a contact angle of 60 ± 1 degrees. Additionally, the ζ of both PS and PVC particles was measured in Milli-Q water to be negative, as reported in Table 1. This negative ζ is indicative of a tendency towards particle repulsion and minimizes the likelihood of agglomeration [42]. The stability of the particles against agglomeration was investigated by measuring their hydrodynamic sizes using DLS over 6 h (Fig. 1a). The SEM-EDS analysis revealed the elemental composition of the PS and PVC nanoplastics. The analysis identified carbon (C) and Gd in the PS particles, and C, chlorine (Cl), and Gd in the PVC particles, as depicted in Fig. 1b. The presence of Gd increased the density of the PS and PVC nanoplastics from 1.05 and 1.38 g/cm^3 to ~ 1.3 and 1.6 g/cm^3, respectively.

Testing the stability of gadolinium in the nanoplastics

To confirm the retention of Gd within the nanoplastic particles, we conducted stability tests for a duration of 6 h in the serum free cell culture medium (for the composition of the culture medium see Methodology, Exposure to nanoplastics) used to establish the co-culture model. The concentration of Gd ions, as well as the nanoplastic number, were quantified at 0 and 6 h using spICP-MS (Supporting Information, Section 2). We recently developed and tested a protocol for the application of spICP-MS to simultaneously measure nanoplastics and the release of metals from them over time [19]. No Gd ions were detected after 6 h in the cell culture medium, aligning with the findings of our prior research [39]. Furthermore, there were no significant changes in particle numbers between the measurements at 0 and 6 h (see Fig. 1c), indicating the nanoplastics' stability against degradation, while DLS data confirmed no notable amount of agglomeration.

Previous studies have indicated that the presence of proteins on the surfaces of particles might expedite the release of ions from metallic nanoparticles through a process known as ligand-mediated dissolution [43]. In the context of Gd-entrapped nanoplastics, it is hypothesized that the adsorption of proteins and metabolites onto their surfaces could potentially lead to leakage of Gd as a result of the affinity of Gd for serum proteins including serum albumin [44]. To ensure that this phenomenon does not induce the release of Gd from the particles, we dispersed the nanoplastics in plasma, and monitored the Gd ion concentration at 0 h and 6 h using spICP-MS. There was no significant difference (*t-test, $p > 0.05$*) in the particle number after 6 h of mixing, and no Gd ions were detectable in the medium throughout the duration of the experiment (Fig. 1d), confirming the stability of the nanoplastics in terms of both Gd retention and particle number for the duration of the BBB exposure studies.

Formation and evolution of the biological corona on the surface of nanoplastics

Fig. 2a illustrates the experiment performed for analysis of the biological corona. Adsorption of biomolecules, such as proteins, onto nanoplastics involves several mechanisms. Electrostatic interactions occur due to surface charges on proteins and nanoparticles, while hydrophobic interactions attract proteins with hydrophobic regions to hydrophobic surfaces, which is expected to be the driving force for biomolecule adsorption onto nanoplastics. Van der Waals forces and hydrogen bonding also contribute, with specific functional groups on nanoparticle surfaces enhancing adsorption through chemical interactions [23]. The structural conformation and flexibility of proteins, along with the ionic strength and pH of the solution, further influence adsorption. Additionally, the size and shape of nanoparticles affect the surface area available for binding, and the dynamic exchange of proteins, known as the Vroman effect, plays an important role in the adsorption process. Understanding these mechanisms is essential for predicting nanoparticle behavior in biological systems [45,46].

TEM images (Fig. 2b) taken after 1 h confirm the formation of a biological corona on the surfaces of both types of particles. This has already been reported for different types of nanoparticles, but less so for nanoplastics [47]. The presence of the corona on the surface of nanoplastics can modify both the size and the ζ of the particles. After a 6-h mixing in plasma, the hydrodynamic diameter of the particles increased to ~ 400 nm (Fig. 2c), indicative of protein adsorption, as was expected. Furthermore, the absolute value of the ζ potential was measured to decrease for PS when they were covered by the biological corona (Fig. 2d). Changes in particle properties such as size or ζ influence the mobility and further transformation of particles within organisms' bodies.

Metabolite corona- For the analysis of the metabolite corona, nanoplastics were incubated in human plasma for 6 h, after which the

Table 1
Physicochemical properties of the nanoplastics applied in this study.

Nanoplastics	Hydrodynamic diameter (nm)	TEM measured diameter (nm)	Chemical composition	Contact angle	Zeta potential (mV)
PS	267 ± 14	258 ± 8	Verified PS	80 ± 2	− 14 ± 1
PVC	255 ± 21	253 ± 13	Verified PVC	60 ± 1	− 15 ± 2

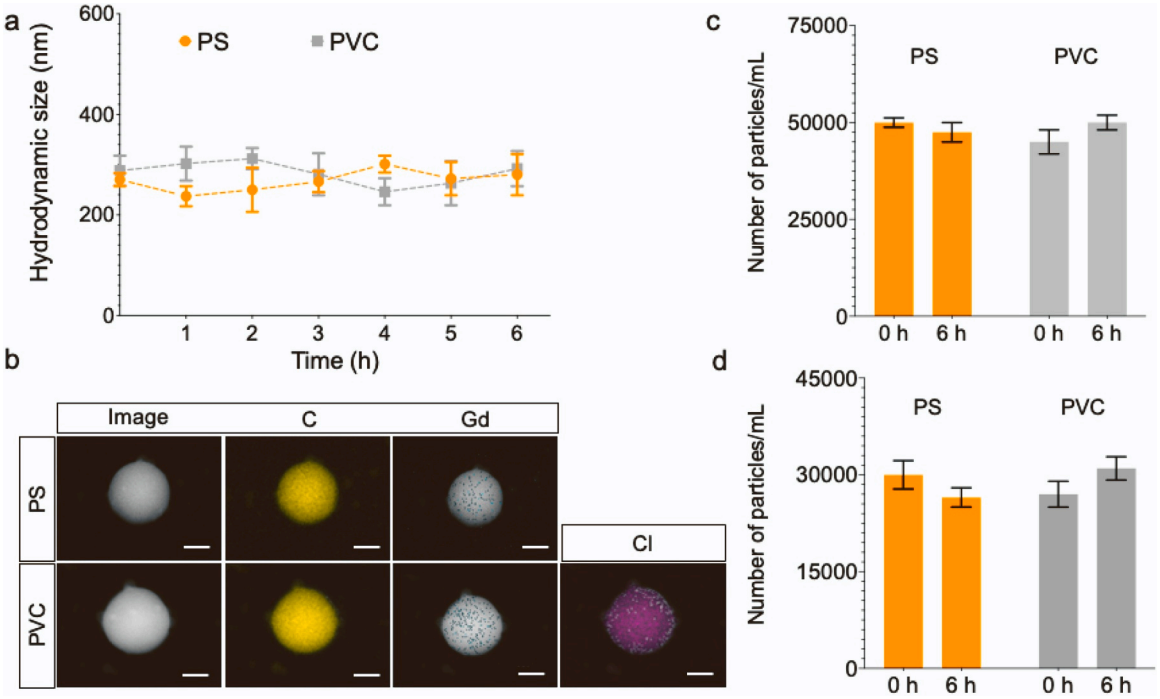

Fig. 1. Characterization of Gadolinium-embedded nanoplastics: a) Agglomeration profiles of PS and PVC nanoplastics in serum-free exposure medium containig diluted human plasma (diluted 10 times in PBS) were assessed using DLS. Over a period of 6 hours, no significant changes (*One-way ANOVA, $p < 0.05$*) in hydrodynamic diameter were observed, indicating the stability of the nanoplastics against agglomeration. **b)** SEM images, along with corresponding EDS elemental mappings, were obtained for PS (showing carbon [C] and gadolinium [Gd] atoms) and for PVC (showing carbon [C], gadolinium [Gd] and chlorine [Cl] atoms). The scale bar represents 250 nm. **c)** The particle number of PS and PVC nanoplastics in the cell culture medium over 6 h. No significant variation was found between 0 h and 6 h (mean ± standard deviation, *t-test: $p < 0.05$*,). **d)** The particle number of PS and PVC nanoplastics in diluted plasma (diluted 10 times in PBS) were quantified at 0 and 6 h of incubation using spICP-MS. No significant variation was found between 0 h and 6 h (mean ± standard deviation, *t-test: $p < 0.05$*.

metabolites adsorbed onto their surfaces were extracted and their variation quantified using liquid chromatography- high-resolution tandem mass spectrometry (LC-HRMS/MS). Approximately 2000 molecular features were identified in the biological coronas of both types of nanoplastics. Compounds categorized as 'leachables', along with other unidentified features, were excluded from the analysis. After subtracting the background signal, 21 identified small metabolites and 26 lipids were selected for further analysis. To benchmark the metabolite concentrations on the nanoplastics, we compared them with untreated plasma (plasma without nanoplastics) and normalized the signal of each metabolite associated with the particles to its corresponding signal in the untreated plasma. The detailed results (Fig. 3) indicate that the nanoplastics exhibit a strong affinity for lipophilic compounds, such as phosphatidylcholines (PC) and lysophosphocholines (LPC), from human plasma. This study is the first to demonstrate how and which types of lipids adsorb to different types of nanoplastics, and it might serve as a starting point for understanding this phenomenon for risk assessment and medical purposes. This data show that the nanoplastics display a selective binding behavior based on the lipophilicity of compounds. In contrast, the nanoplastics showed a markedly lower binding affinity for polar, small molecular weight compounds, such as amino acids, suggesting that the tested nanoplastics favor lipophilic interactions. This preferential binding suggests that nanoplastics could accumulate in lipid-rich tissues and potentially interfere with lipid-based biological processes in the brain if they can pass through the BBB. Understanding this behavior is crucial for evaluating the potential health risks posed by nanoplastics, as it indicates a specific pathway of interaction and accumulation within organisms.

While the observed variation between replicates was considerable, no significant differences were found in the metabolite profiles on the surfaces of PS and PVC nanoplastics (as determined by *ANOVA, $p < 0.05$* in all cases). This observation has far-reaching implications. The metabolites adsorbed onto the surface of nanoplastics can significantly affect their biological fate, influencing factors such as biodistribution within the human body and potential for degradation over time [48]. The absence of a notable difference in metabolite adsorption between the two different nanoplastic compositions suggests that the chemical composition of nanoplastics may play a relatively minor role in metabolite adsorption. Note taht these results can not be extrapolated to all types of nanoplastics as we have only investigated two types of plastic particles. This could pave the way, however, for the development of a general framework for grouping these particles for risk assessment purposes, as employed for other nanomaterials [49]. Such an approach would categorize nanoplastics based on their behavior in biological systems, supporting read-across predictions. This allows researchers to infer properties or effects of one substance based on data from a similar substance that is better understood, thereby circumventing the need for exhaustive studies on the target substance. This approach is particularly advantageous for assessing the risks associated with various types of nanoplastics where toxicological data is scarce or non-existent. It is important to note, however, that the protein component of the biological corona, in addition to metabolites, plays a critical role in the interactions and subsequent behavior of nanoplastics in physiological conditions [23]. This suggests that while metabolite adsorption patterns may be similar across different nanoplastics, the complete biological corona [25]– including proteins – must be considered to fully understand and predict the biological behavior of these materials.

Protein corona- Following incubation, proteins comprising the corona were eluted and their abundances quantified using TMT Tandem Mass Tag (TMT)-based quantitative proteomics [50]. The abundance of proteins in the corona was then assessed relative to their abundance in undiluted human plasma. A total of 268 proteins were reliably identified as being present in at least one of the biological coronas recovered from the surfaces of the nanoplastics. The average log2 fold changes (FCs) and

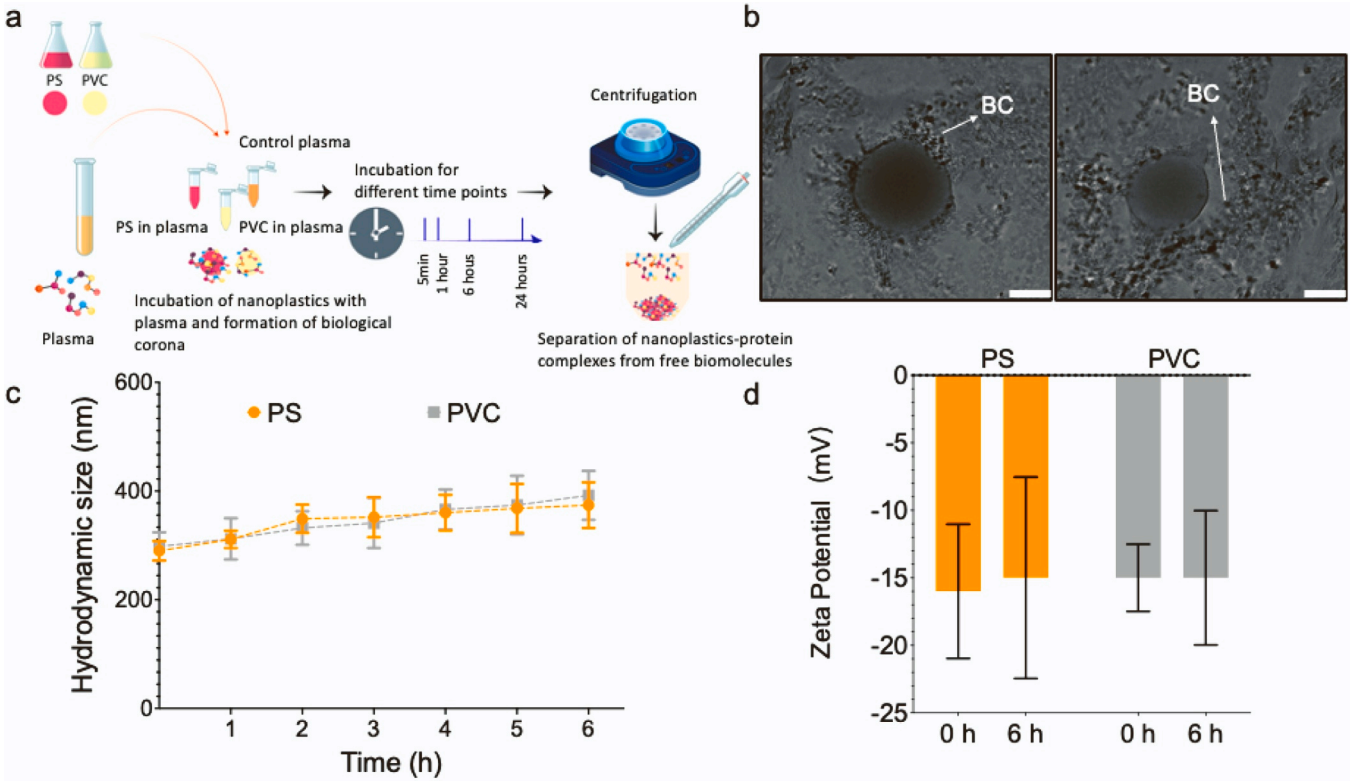

Fig. 2. Formation and characterization of the nanoplastic-biological corona (BC) complex. a) A schematic diagram illustrating the incubation of nanoplastics in plasma followed by the extraction of particles for analysis. **b)** TEM images confirming the formation of the biologicl corona on the surface of the nanoplastics after 1 h mixing in plasma. **c)** The change in the hydrodynamic size of the nanoplastics when incubated in plasma over a 6 h , and **d)** ζ measurements of the particles at 0 and 6 h (mean ± standard deviation, *t-test:* $p < 0.05$).

adjusted p-values were calculated (see Additional file proteome: Table 1), revealing that 241 proteins were significantly enriched (adjusted *p-value* ≤ 0.05) on either PS or PVC nanoplastics. Additionally, the reliably identified proteins were analyzed using Principal Component Analysis (PCA), which revealed only minor differences in the protein coronas of the two nanoplastics (Fig. 4a). Time-dependent formation of the protein corona was observed on both PS and PVC nanoplastics (Fig. 4b). To further analyze time-dependent protein associations with the nanoplastics, Weighted Gene Correlation Network Analysis (WGCNA) was employed. This network analysis identified five modules of co-abundant proteins that are named by colors (Fig. 4b). We then assessed the temporal correlation of these modules and their relationship with combined time points for both types of particles (Fig. 4c). The correlation values obtained from the analysis indicated the propensity of proteins within a module to become enriched (correlation > 0) or depleted (correlation < 0) over time. Notably, the two modules in Fig. 4d exhibited distinct correlation patterns: the blue module showed a clear trend of time-dependent protein enrichment, whereas the brown module reached peak enrichment at the 1-h and 6-h time points.

Subsequently, we identified putative 'key drivers'—proteins that exhibit high connectivity within their respective modules and show strong association with a specific trait, i.e., with the different time points. Using the combined time points for both PS and PVC nanoplastics as the trait, we were able to pinpoint particle-specific key driver candidates. The top 10 key drivers were selected based on their combined absolute module membership and their significance with respect to the protein-trait relationship (see Additional file proteome: Tables 2–5). Remarkably, the top 10 proteins were consistent across both nanoplastic types in the modules of interest, as shown in Fig. 4c. This indicates that similar proteins adhere to both PS and PVC nanoplastics. Within the blue module, which showed a pattern of time-dependent enrichment, notable candidates included apolipoproteins such as APOL1 and APOB. In contrast, the brown module, which was predominantly enriched at 1 h and 6 h , included key coagulation factors like F2, F9, and F10. It has been previously documented that nanoparticles exhibit an affinity for apolipoproteins, with evidence showing that hydrophobic materials tend to adsorb apolipoproteins to a greater extent than hydrophilic ones, which preferentially bind more abundant proteins such as albumin, fibrinogen, and IgG [51]' [52]'[53]. Our findings corroborate these observations, indicating that different types of nanoplastics predominantly adsorb similar protein types over time. The presence of specific proteins on nanoplastics can dictate their biodistribution within organisms, suggesting that various nanoplastic types could share a similar biological fate in humans. These insights lend support to the feasibility of a grouping approach for nanoplastics and highlight the potential for employing read-across strategies in risk assessment.

Permeability of in vitro BBB model to nanoplastics

The differentiation of human induced pluripotent stem cell (iPSC)-derived endothelial cells (iECs) and astrocytes was characterized. The details of this characterization are illustrated in Fig. 5a and d. To investigate nanoplastics trafficking and translocation, it is essential to first confirm that the BBB model has successfully formed a monolayer with intact tight junctions. Initially, the formation of a BBB cell monolayer was verified using a TEM method, as previously established [54]. The TEM images confirmed the formation of a monolayer of induced pluripotent stem cell-derived iECs on the apical side of the Transwell system (Fig. 5b). The convergence of adjacent cell boundaries, as observed in Fig. 5c, suggests a tight sealing of the paracellular space, indicative of the presence of tight junctions. Consequently, this structural integrity inhibited the paracellular transport of nanoplastics. The mature astrocytes developed a characteristic star-like morphology and exhibited a high level of glial fibrillary acidic protein (GFAP) expression,

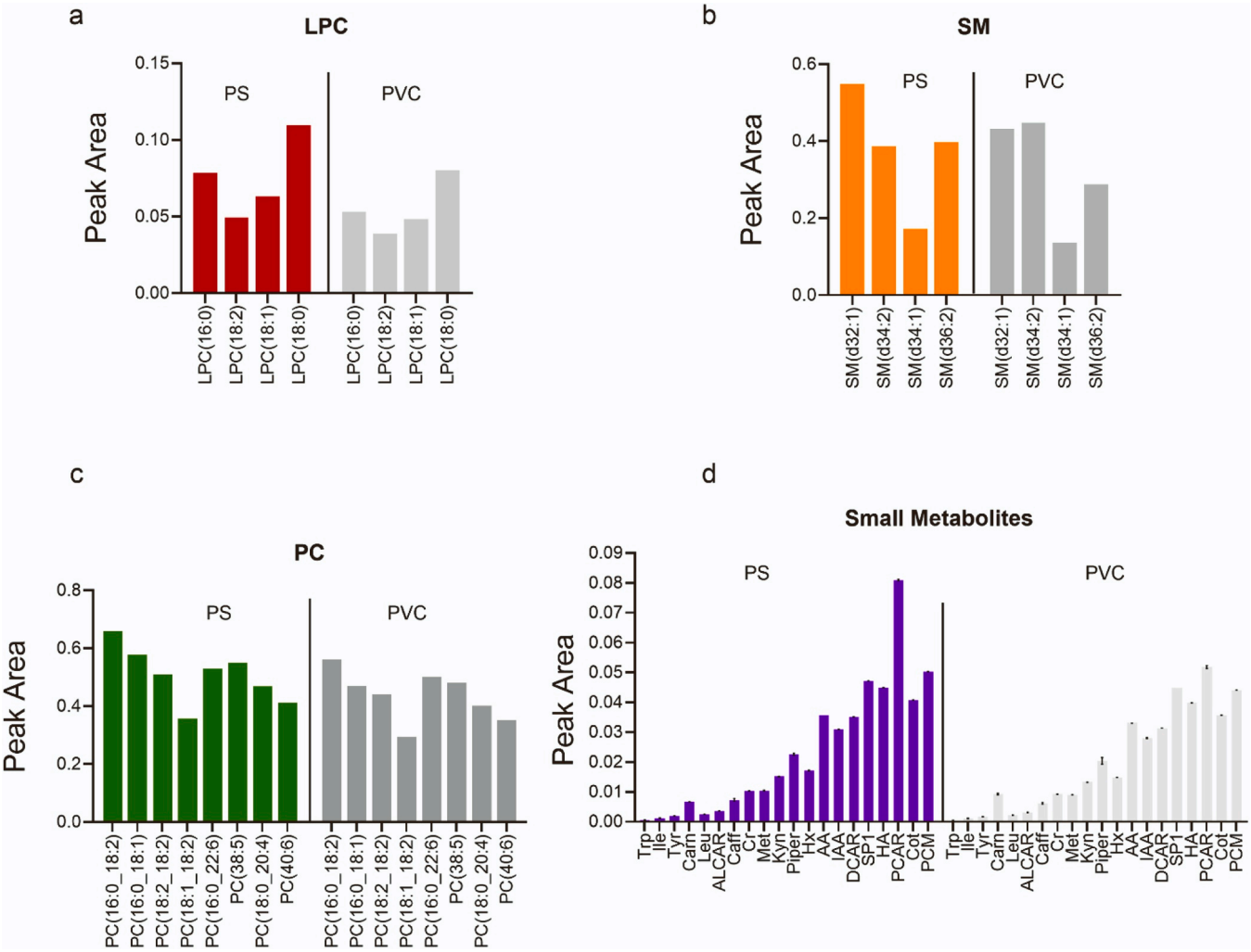

Fig. 3. : Comparative analysis of lipid and small metabolite binding to nanoplastics. The normalized peak area ratios of bound lipids and small metabolites to PS and PVC nanoplastics relative to untreated controls. **a)** Lysophosphatidylcholines (LPC) show a higher affinity for PS (red bars) as compared to PVC (gray bars). **b)** Sphingomyelins (SM) demonstrate similar binding profiles for both PS (orange bars) and PVC (gray bars). **c)** Phosphatidylcholines (PC) bind slightly more to PS (green bars) than to PVC (gray bars). **d)** Small metabolites, including amino acids and carbohydrates, display varying degrees of association with PS (purple bars) and PVC (gray bars), with some showing a preference for PS (results show the mean ± standard deviation).

as shown in Fig. 5d. While the S100b protein was expressed in all astrocyte cells, not all astrocyte cells were positive for GFAP. The astrocytes also expressed transporters, including SLC1A2 and SLC1A3 (Fig. 5d). To investigate potential differences in induced pluripotent stem iECs cultured in both mono-culture and co-culture with astrocytes, immunocytochemistry (ICC) staining and permeability tests (Fig. 5c and e) were performed. The expression of the tight junction protein ZO-1 and endothelial marker CD31 showed no differences between the two culture conditions. In the permeability tests, where lower permeability indicates a more effective cell barrier, the results demonstrated that permeability (calculated as the permeability coefficient, PE-value) was four times higher for LY (0.4 kDa) compared to dextran molecules. Comparing co-cultures and monocultures, no significant differences in permeability were observed. However, there were subtle differences in permeabilities detected when dextran molecules were used, resulting in co-cultures having tighter barrier properties. Therefore, we selected the co-culture model for subsequent experiments.

Cells were treated with a concentration of 5 μg L^{-1} of either pristine PS and PVC nanoplastics or those covered with a biological corona provided from the previous section after incubation of particles with human plasma for 6 h (Fig. 6a). This specific nanoplastic concentration was selected to represent the levels of nanoplastics expected to be found in the environment, as reported in the literature [55]. The duration of cell exposure to nanoplastics was set at 2 h. After the exposure, the cell insert was washed with PBS, and the cells were fixed for TEM imaging. Although incorporating Gd into the polymeric particles was intended to enhance their visibility under TEM, the metal's density proved insufficient for clear intracellular distinction. However, we did observe structures resembling nanoplastics within the cells that were exposed to pristine nanoplastics, as shown in Fig. 6b. These structures were absent in the control group of unexposed cells. Notably, PS nanoplastics were identified in the interstitial space (deattached part of the cells from the filter) between the iECs cells and the filter membrane (Fig. 6c), indicating the potential for these particles to traverse through the cellular layer. The presence of membrane ruffles and cups (Fig. 6d) suggests that PS nanoplastics may traverse the BBB through mechanisms akin to macropinocytosis. Similar phenomena have been noted for other types of nanoparticles in medical research contexts [56], [57], [58]. Within the BBB, the cerebral access of small molecules is primarily facilitated through passive diffusion or active transport mechanisms. However, in the case of nanoparticles, it is reported that transcytosis is the predominant route for entering the brain. This process encompasses endocytosis, intracellular vesicular trafficking, and subsequent exocytosis, enabling nanoparticles to cross the BBB.

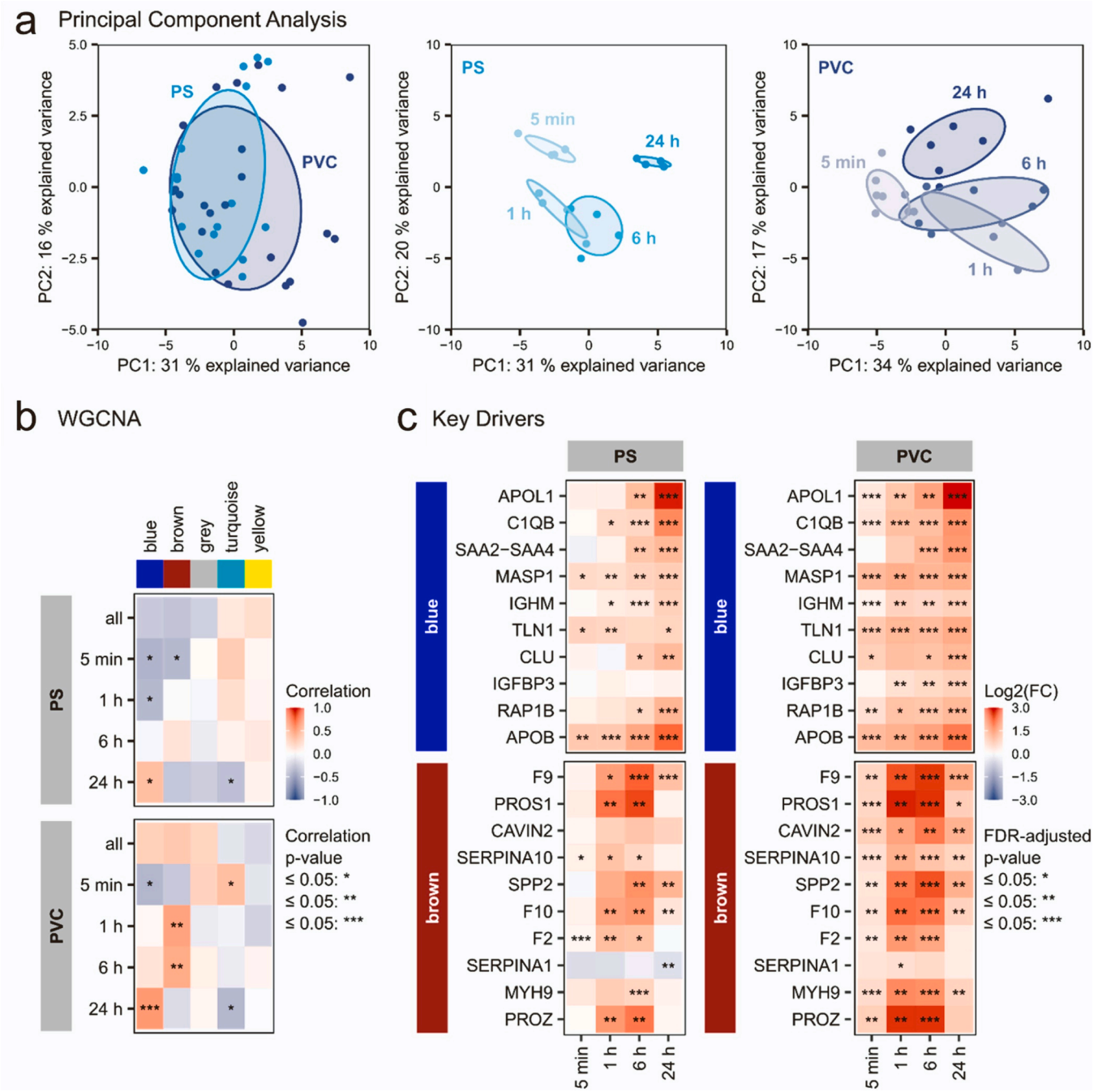

Fig. 4. Protein corona composition on PS and PVC nanoplastics. a) Identification of proteins constituting the corona on PS and PVC nanoplastics after exposure to human plasma for 5 min, 1 h, 6 h, and 24 h. The relative abundance of proteins is measured against their presence in pure human plasma, with the depicted values indicating either enrichment (log2 fold change [Log2(FC)] > 0) or depletion (Log2(FC) < 0) compared to the pure plasma baseline. Proteins with enriched abundances are considered constituents of the protein corona. A Principal Component Analysis (PCA) of the log2(FCs) indicated slight differences between the two types of nanoplastics yet revealed a clear time-dependent composition of the protein corona for both nanoplastic types. **b)** Through Weighted Gene Correlation Network Analysis (WGCNA), five modules of co-abundant proteins were discerned. Specifically, the blue module represented proteins increasingly enriched over time on both nanoplastics, while the brown module showed proteins predominantly identified in the corona at 1 h and 6 h. **c)** The top 10 key drivers within these modules were determined based on their combined absolute module membership and protein-trait significance scores, considering all time points for both PS and PVC nanoplastics.

Finally, it is crucial to evaluate the impact of various treatments on cell viability, as this factor can significantly influence the trafficking and translocation of nanoplastics. We have performed a cell viability assay using DAPI (4′,6-diamidino-2-phenylindole) staining on iECs and astrocytes after exposure to 5 μg L^{-1} of either pristine PS and PVC or biological corona coated nanoplastics. It's important to note that DAPI binds strongly to DNA, serving as a marker for cell nuclei in dead cells within our experimental set up, as the cells were not fixed prior to quantification. Consequently, cell viability was determined by counting the total number of cells and observing for any morphological changes' indicative of cell death. The cell viability was found to range between 95 % and 99 %, with no significant differences detected between the various treatments, as shown in Fig. 6e.

To substantiate our observations of nanoplastics internalizing within BBB cells and potentially passing through iECs, we implemented a novel approach to quantify the number of particles inside both iECs and

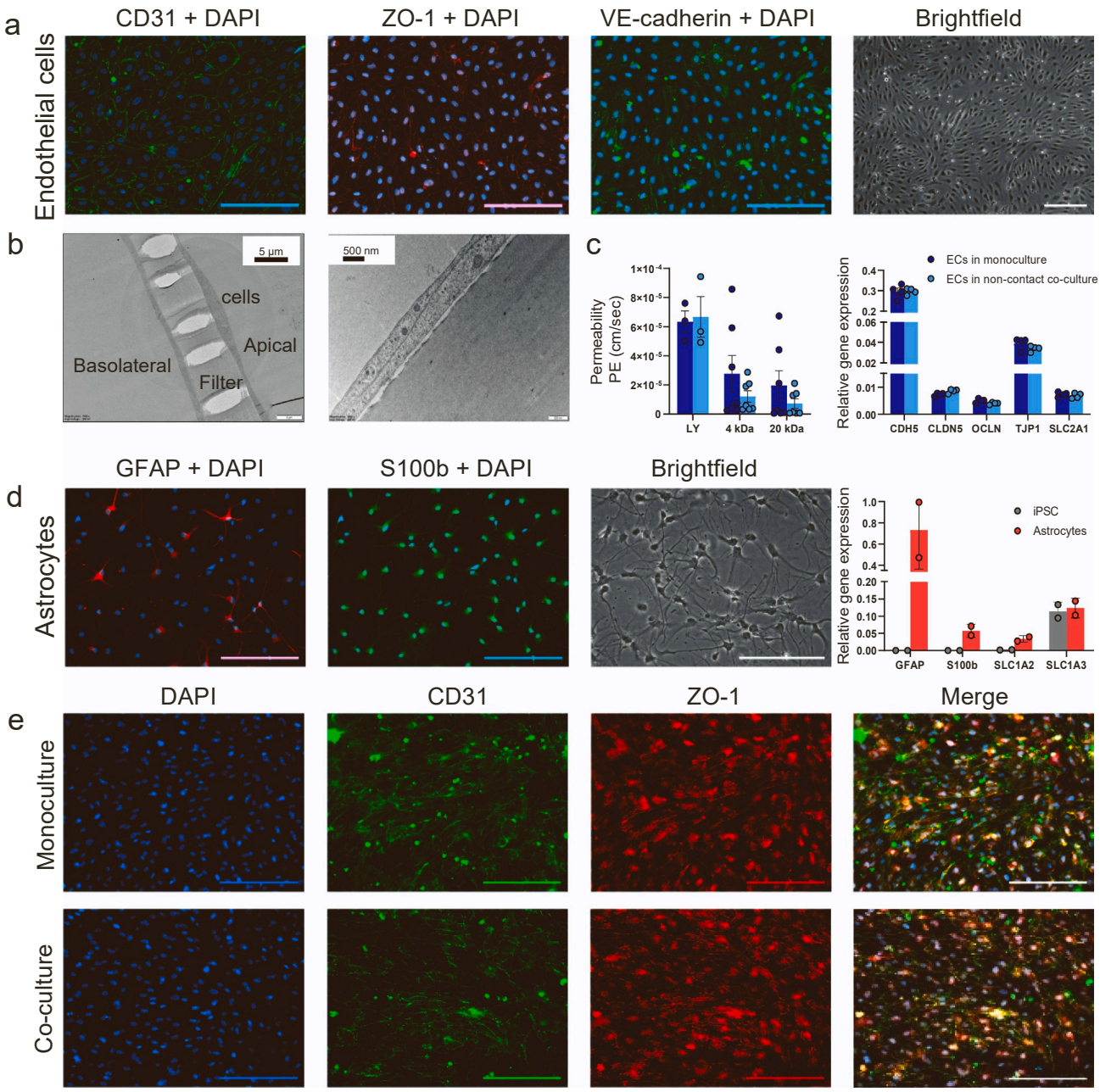

Fig. 5. Cell culture and permeability assessment. a) ICC staining of endothelial cells (iECs) for VE-cadherin, ZO-1, CD31 and DAPI and brightfield image of iECs in ECGM MV2 medium. **b)** A TEM image displaying a monolayer formation of endothelial cells on the filter (left) and a TEM image highlighting the tight junctions between endothelial cells (right). **c)** Permeability (mean and standard error of the mean or SEM) and relative gene-expression (mean and standard deviation, SD) of iECs in culture model set ups. **d)** Astrocyte characterization: ICC staining with S100b, GFAP and DAPI, brightfield image of astrocytes and relative gene expression (mean and SD) of the astrocytes compared to hiPSCs. **e)** ICC staining of iECs for DAPI, CD31 and ZO1 in monocultures and non-contact co-cultures with astrocytes.

astrocytes. Utilizing Gd as a marker, our method enables the quantification of individual nanoplastics within cells [30]. This contrasts with previous methodologies that primarily focused on quantifying the mass of particles [59]. In the field of nanotoxicology, determining the accurate count of particles is crucial [36]. The volume-specific surface area of particles, a factor that can amplify potential hazards, is directly proportional to the number of particles [60]. To quantify the amounts of PVC and PS nanoplastics within the cells, we employed spICP-MS[36]. The results revealed that both PS and PVC nanoplastics were internalized by iECs and astrocytes, as shown in Fig. 7. Given the design of the co-culture model, whereby the astrocytes were not in direct contact with the inserts, the only way that particles could be taken up by the astrocytes was if they first crossed the iEC layer into the well medium. This finding suggests that both PS and PVC can permeate the *in vitro* BBB model. This finding can not be directly transferred to *in vivo* condition, considering the complexity of the organisms bodies.

Notably, pristine PVC nanoplastics were found to be more prevalent within both cell types than pristine PS nanoplastics. Given that both types of particles have comparable shape, size, and surface charge, this observation suggests that the chemical composition of the pristine nanoplastics may be a critical factor in determining their cellular uptake. Thus, it is essential to mimic real exposure conditions when conducting nanoplastic studies for safety purposes and to consider all influential parameters, such as the biological corona, to draw conclusions that closely reflect reality rather than relying on experiments with pristine particles, which do not represent realistic scenarios. Chlorine

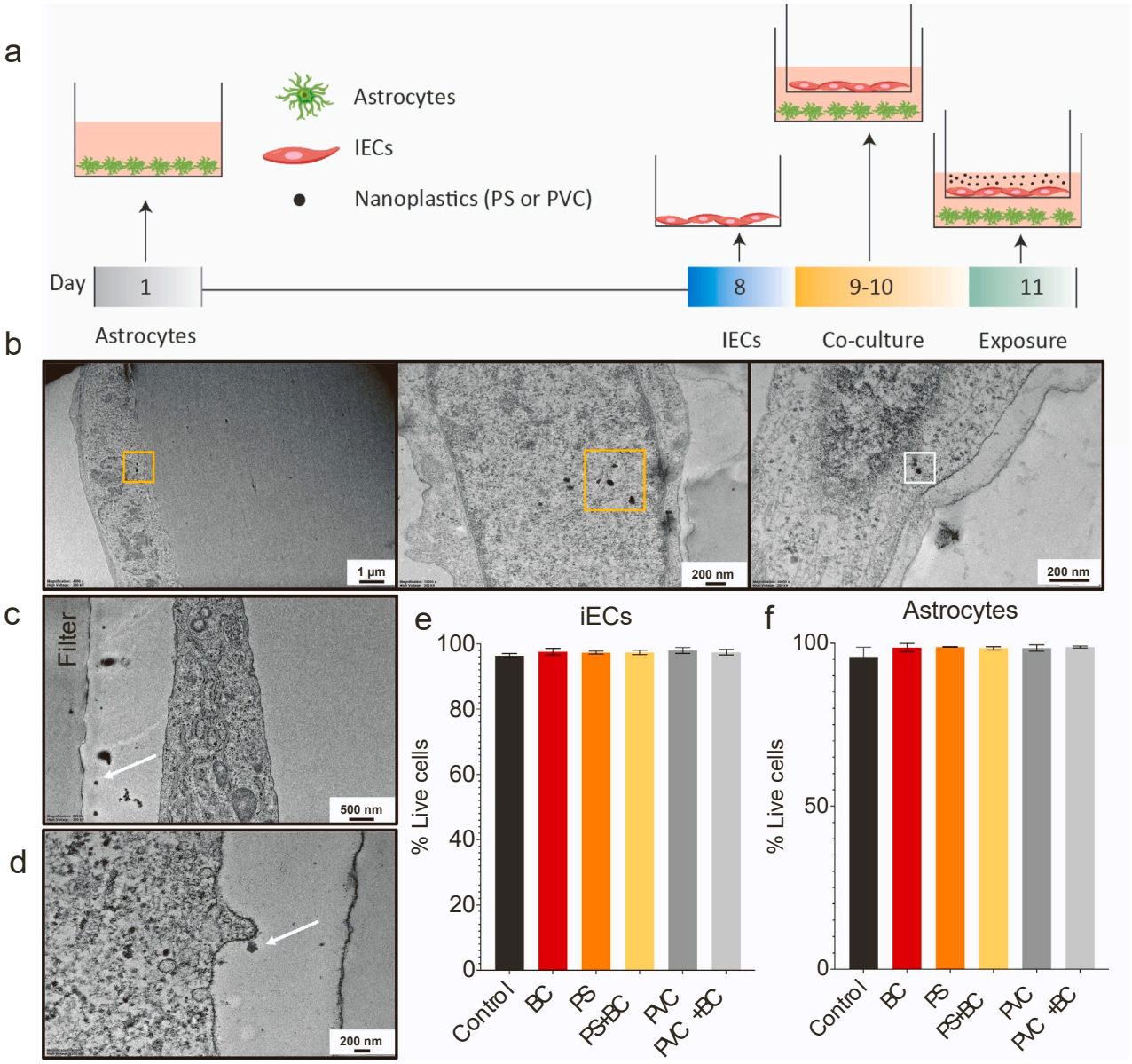

Fig. 6. Exposure of BBB to PS and PVC nanoplastics. a) Schematic illustration of cell culture and the exposure of the BBB model to nanoplastics. **b)** Possible internalization of nanoplastics by iECs following a 2-h exposure. **c)** Nanoplastics were found between the filter and the iECs cells in the part where the cells were deactached from the filters, indicating that nanoplastics could pass through the iECs. d) Emergence of membrane ruffles facilitating nanoplastic uptake via macropinocytosis. Cell viability of **e)** iECs and **f)** astrocytes exposed to 5 µg/L of PS and PVC nanoplastics or biological corona (BC) coated nanoplastics (mean ± standard deviation based on six replicates).

increases the density of PVC relative to PS. The density of Gd-labeled PVC is 1.7 g cm^3, compared to 1.3 g cm^3 for PS. It is also likely that more PVC settled onto the cells during the exposure, resulting in increased cellular uptake. This highlights the importance of adopting different protocols for nanotoxicity testing of nanoplastics, rather than using protocols developed for chemicals where a homogeneous solution is expected, while nanoplastics exhibit different and dynamic behavior in the exposure medium [37]. Our results, however, indicated a significant decrease in the cellular uptake of PVC particles when they were coated with the biological corona (Fig. 7a, b). This finding suggests that the biological corona and the variations in its composition on the surface of nanoplastics, or specific patterns of biological corona formation, could significantly influence the uptake of nanoplastics within the BBB [61], [33]. A previous study on nanoparticles showed that the formation of protein corona can reduce overall particle density, resulting in an apparent decrease in size upon corona formation, which was corrected when density differences were accounted for using a core-shell model with different densities [62]. Formation of the biological corona could counteract some of the increased density provided by the Gd entrapment in the particles.

It is plausible that the presence of a biological corona may hinder the penetration of nanoplastics in BBB within living organisms. Biological coronas primarily drive particle uptake via receptor-mediated endocytosis (RME). However, in the absence of the biological corona, non-specific uptake and membrane damage may occur, leading to higher overall uptake [63]. Our results diverge from previous studies that indicated nanoplastics penetrate into the same BBB model at high concentrations [33]. This discrepancy could be attributed to differences in the methodologies applied as well as variations in the size and type of nanoplastics. Previous studies often relied on modeling approaches [33] or utilized fluorescent labeling of the particles surface [34], which may not accurately replicate the behavior of non-labeled nanoplastics in

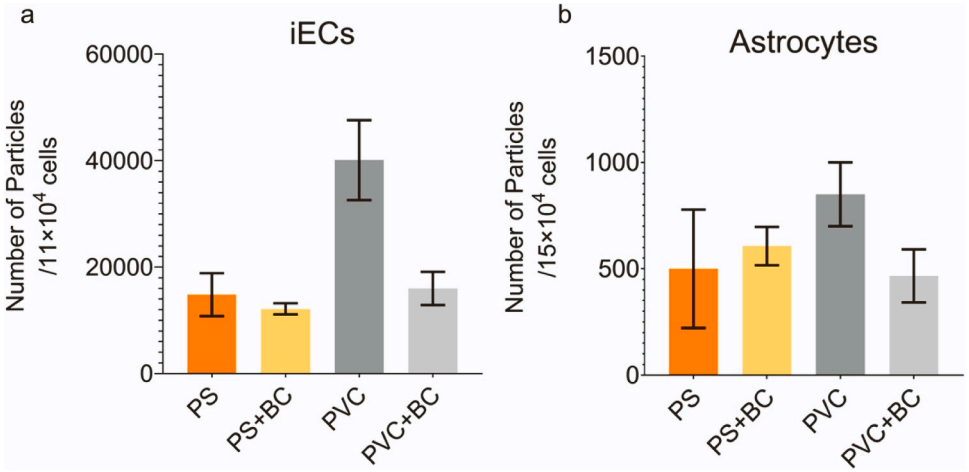

Fig. 7. Number of nanoplastics determined to be present in the cells following exposure for 2 h to 5 μg L^{-1} of 250 nm PS or PVC nanoplastics. a) Number of PS and PVC nanoplastics found within iECs, pristine and biological corona (BC)-coated, respectively. **b)** Number of PS and PVC nanoplastics located in astrocytes. Note that to reach the astrocytes, the nanoplastic particles had first to traverse the iECs, and thus the exposure concentration was lower in this case. The presence of nanoplatics in the astrocytes is evidence of transcytosis of nanoparticles through the iEC cells / the BBB (mean ± standard deviation, *One-way ANOVA*, $p < 0.05$).

biological systems [36]. The distinct behavior between PVC and PS nanoplastics in cellular uptake underscores the importance of the chemical composition of nanoplastics in determining their bio-interactions. The reduced uptake of PVC particles coated with a biological corona highlights the significant role that surface modifications or corona coatings play in nanoplastic interactions with cells. This insight can have implications for biomedical applications and suggests that the biological corona might act as a protective barrier, potentially reducing the risk of nanoplastic uptake.

Conclusion

This study investigated the interactions between nanoplastics and biological matrices through the employment of advanced analytical methodologies specifically designed for nanotechnology applications. These methodologies include the entrapment of Gd in polymeric matrices for quantification and characterization, along with the utilization of sp ICP-MS and SEM-EDS. Additionally, a novel protocol for observing nanoplastics inside cells using TEM was applied. A notable finding is that regardless of their chemical composition, nanoplastics selectively bind lipophilic compounds from plasma. The proteomic analysis underscores a dynamic temporal attachment of specific proteins to nanoplastics. Remarkably, despite compositional differences between PS and PVC nanoplastics, similar proteins seem to dominate their respective initial coronas. Furthermore, the study establishes that nanoplastics, whether in their pristine form or coated with a biological corona, can permeate the BBB. The chemical composition did not yield significant alterations in the BC; however, it did prompt variations in cellular uptake in the absence of the biological corona. Differences in particle density of plastics could be the cause of the variations in uptake. This may stem from differences in the settling behavior of the particles due to variations in density. The presence of a biological corona not only decreased cellular uptake but also minimized the variation in cellular uptake between PVC and PS nanoplastics, thereby smoothing out the effect of chemical composition. The findings carry significant biomedical implications and also underscore the urgent need for customized risk assessments.

Materials and methods

Chemicals and materials

All chemicals, unless otherwise stated, were reagent grade and obtained from Sigma–Aldrich. Milli-Q water was provided by a Millipore® filtration system (RiOs™ Essential 16 Water Purification System). The PS (250 nm PDI: 0.2) and PVC (250 nm, PDI: 0.1) nanoplastics were custom designed by our group and synthesized by cd-bioparticles (NY 11967, USA) according to our specifications. Custom Gd^{+3} was incorporated into the particles. The quantity of Gd in the particles was 9.7 %-11 % as measured by ICP-MS. Gd was chosen due to its rarity in nature, enabling easy detection and quantification using ICP-MS without interference, and the nontoxic nature of Gd at low concentrations (up to 10 mmol L^{-1}) [19], [64]. Additionally, Gd slightly increased the optical density of the particles, aiding in imaging using TEM in biological media.

Observation of nanoplastics using transmission and scanning electron microscopy

The chemical composition of the Gd-entrapped nanoplastics was examined using SEM- Energy Dispersive X-Ray (EDX) analysis. In the presence of Gd, characteristic X-ray peaks should typically occur between 0.9 and 1.2 keV. The samples were observed using a Field Emission (Schottky type) SEM. An acceleration voltage of 4 kV was applied under high vacuum conditions (pressure, $P < 2$ mPa) during the observation. Micrographs were captured with an InLens secondary electron detector to enhance spatial resolution and visualize all particles of interest. The imaging of nanoplastics in cells and nanoplastic-protein complexes was conducted using a TEM (JEOL JEM-2100 F, JEOL Corp., Tokyo, Japan) operating at 200 kV following the previously described method [39].

Incubation of nanoplastics in plasma

The nanoplastics were dispersed in a small volume of physiological buffer saline (PBS, 100 mg L^{-1}) and then incubated in human plasma (×10 diluted with PBS) to achieve a final particle concentration of 10 mg L^{-1}, following the previously described method [19]. Note that the concentration of the particles was selected to facilitate easy quantification and identification of the biomolecules forming the corona. For cellular exposure, we used a lower particle concentration to better represent real-exposure conditions and selected a corona-formation time of 6 h. The samples were placed on a rotator at 37 °C and incubated for different times: 5 min, 1 h, 6 h, and 24 h. After each incubation period, unbound proteins and metabolites were removed through a stepwise washing process: (i) 1 ml of PBS was added to the sample and

centrifuged at 2500 ×g and 4 °C for 10 min, (ii) the supernatant was, and the previous washing step was repeated twice, and (iii) 1 ml NH_4HCO_3 was added to the resulting pellets. Four replicates were prepared for each time point. The supernatants, containing free proteins and possibly any released Gd, were used to measure the concentration of Gd released from the particles using spICP-MS. The resulting pellets were re-dispersed in PBS. The nanoplastic-protein complexes were characterized in terms of size and charge using DLS, and shape using TEM. The number of particles was measured using spICP-MS, as it has been demonstrated to effectively measure metals associated with nanoplastics [19]. The remaining samples were stored at −80 °C for further analysis.

Plasma metabolite isolation and non-targeted metabolite profiling

A detailed description of the isolation procedure and method is reported in the supporting information Section 3. The samples were analyzed using reversed phase liquid chromatography (RPLC) and high-resolution mass spectrometry, as described previously [65]. Briefly, the samples were centrifuged at 700 × g and 4 °C for 5 min and the supernatants were collected into conical glass vials. Six replicate samples were made for both nanoplastic types (PS and PVC). The sample solution (2 μL) was injected onto a RP column (Zorbax Eclipse XDBC18, 2.1 × 100 mm, 1.8 μm, Agilent Technologies, Palo Alto, CA, USA) that was kept at 40 °C. Mass spectrometry was equipped with a heated electrospray ionization probe (ESI). The positive ionization mode was used to acquire the data in profile mode. A solvent blank was injected six times at the beginning of the sequence to equilibrate the analytical platform. The LC-MS data alignment, molecular feature finding, and peak picking was done using Compound Discoverer 3.3. software (Thermo Scientific, Bremen, Germany). Compounds that were found in PVC and PS extracts in the absence of plasma (blanks) were subtracted from the data. Compounds that were successfully identified by MS/MS using an in-house and *m/z* Cloud spectral library (small molecules) or LipidSearch software (lipids, Thermo) on the treated nanoplastic particles and/or plasma background were used for calculations.

Untargeted proteomics to evaluate the serum-acquired protein coronas

A detailed description of the method is reported in the supporting information Section 3. Protein concentrations were determined using the DC Protein Assay (BIO-RAD) according to the manufacturer's instructions. The LC –MS/MS analysis was conducted using TMT and a paramagnetic bead approach as described before [66]. The obtained raw data were processed against the UniProt reference proteome of *Homo sapiens* (6 December 2021) using Proteome Discoverer 2.5. Protein fold changes (FCs) of the protein corona samples were calculated against the protein abundances obtained for pure human plasma, resulting in values reflecting either enrichment or depletion of proteins due to exposure of nanoplastics to human plasma. To identify proteins being attached onto the nanoplastics in a time-dependent manner (i.e., not present at early timepoints due to low abundance or not present at longer times due to low affinity), a Weighted Gene Correlation Network Analysis (WGCNA) [67] was applied as described before [68]. The top 10 key drivers, which are the proteins found in the coronas of PS and PVC nanoplastics to be dependent on the incubation times, were identified based on their summed absolute protein-trait significances (Additional file proteome: Table 2) and module memberships (Additional file proteome: Table 3). This was done for all available modules and conditions (Additional file proteome: Table 4) and visualized using the corresponding gene names (Additional file proteome: Table 5) for the relevant modules with significant correlations.

Cell cultures

Human induced pluripotent stem cells. The human induced pluripotent stem cell, Cellartis® Human iPS Cell Line 18 (Takara Bio, Cat: Y00300) (hiPSC), was used for the differentiation of astrocytes and endothelial cells (Supporting Information, Section 4) [69]. Human iPSC-derived endothelial cells (iECs) were differentiated from hiPSC according to the previously described protocol [69]. The astrocyte differentiation was induced following the protocol published by Krencik & Zhang [70] with modification as introduced by Oksanen et al. [71] (Supporting Information Section 4). The detailed methods for immunocytochemistry (ICC), the real-time qPCR are described in the supporting information Section 4.

BBB Model Setup. The cell culture model used in this study consisted of a co-culture of iECs and astrocytes. The characterization was made for a monoculture of iECs and a co-culture of iECs with astrocytes. The steps involved in development of the co-culture model are described in the supporting information (Supporting information Section 4). Two days after co-cultures of iECs and astrocytes were initiated, the nanoplastic exposure experiments were conducted. For characterization of the monoculture model, the astrocytes were left out.

Permeability assay. The permeability tests for mono- and co-cultures were made with two sizes of fluorescently labeled 0.5 mg ml^{-1} Dextrans, 4 kDa fluorescein isothiocyanate (FITC)-Dextran (Sigma, Cat: 46944–500MG-F) and 20 kDa tetramethylrhodamine (TRITC)-Dextran (Merck, Cat: 73766–1 G) and 0.4 kDa Lucifer Yellow CH dipotassium salt (LY) (Sigma-Aldrich, L0144) of 0.1 mg ml^{-1} two days after starting the co-cultures (further details provided in supporting information Section 4). As a control for the permeability calculations, Matrigel coated inserts without cells were used. Samples (150 μl) were collected from the wells at 20, 40, 60, 75 and 90 min after adding the Dextran or LY solution. The equivalent volume of fresh medium was then added to maintain a constant volume c. At the 90-minute time point, additional samples from the insert were collected. Afterwards the samples were prepared for ICC and real-time quantitative polymerase chain reaction (RT-qPCR). For RT-qPCR, the iECs were detached from inserts with TrypLE Express, pelleted and stored at −70 °C for RNA extraction. The inserts were later stained with ZO-1 and DAPI, and RT-qPCR was performed for the genes CDH5, CLDN5, OCLN, TJP1 a SLC2A1 (more detailed information on the list of primers is provided in Table S2 in the supporting information Section 4). The permeability efficiency (PE) was calculated as described previously [72] and presented as PE (cm/sec). In brief, PE was determined using the formula: $1/PE = 1/mc - 1/mf$, where mc is the slope of the cleared volume plotted against time for inserts containing iECs and mf is the slope of the cleared volume plotted against time for inserts without iECs.

Exposure to nanoplastics

Cells were exposed for 2 h to a concentration of 5 μg L^{-1} of either pristine PS or PVC nanoplastics or the nanoplastics with their acquired biological corona. The nanoplastic exposure experiment was conducted in the co-culture model with iECs and astrocytes. Six different treatments were tested on the transwell model. The treatments used were as follows: 1) co-culture medium (75 % of astrocyte differentiation medium + 25 % human endothelial serum free medium with 1x B27, 10 ng/ml bFGF and 0.55 μM hydrocortisone; see supporting information Section 4 for full composition of the medium) without cells and particles as a control, 2) plasma proteins in PBS (*10) as a control mixed with co-culture medium, 3) pristine PS nanoplastics in co-culture medium, 4) PS nanoplastics pre incubated in human plasma for 6 h (PS-BC), 5) pristine PVC nanoplastics in the previously described co-culture medium, and 6) PVC nanoplastics pre incubated in human plasma (PVC-BC). The pre-incubated nanoplastics in human plasma underwent a process where the particles were initially mixed with the plasma, followed by isolation and subsequent resuspension in the expeosure medium to form the biological corona (BC). The number concentration of the particles were equal for both nanoplastics. Fresh co-culture medium was added to the wells, and treatment solutions were applied to the inserts. Four

replicates were used for each treatment. One control insert was taken for TEM analysis (to observe tight junctions) at the beginning of the experiment, and after 1 h of treatment, one insert per treatment (PS, PS-BC, PVC, PVC-BC) was taken for TEM analysis to observe the localization of the particles. After 2 of treatment, the wells and inserts were washed, and cells were detached (see supporting information Section 4). Each sample was divided into smaller samples for further analysis.

Cell viability assay

To determine if the nanoplastic treatments affected the viability of the cells, we collected samples from iECs and astrocytes at the end of the exposure experiment. The samples were incubated with the nuclear dye DAPI (4′,6-diamidino-2-phenylindole dihydrochloride, Sigma, Cat: D9542) at a ratio of 1:2000 for 5 min at room temperature. Before the analysis, quality control was performed with CytoFLEX Daily QC Fluorospheres to ensure that the system is optimized and ready to produce accurate and precise results (Beckman Coulter, cat: B53230). The violet laser at 405 nm was used to detect DAPI from the collected samples.

Cell fixation and sectioning

To examine the localization of nanoplastics within cells by TEM, samples were fixed using 2.5 % glutaraldehyde in 0.1 M phosphate buffer at pH 7.4 and sliced into small and thin sections using an ultramicrotome (Supporting information section 5). The resulting sections were observed using TEM.

Data analysis

The graphs were generated using GraphPad Prism version 10.2.0, GraphPad Software, Boston, Massachusetts USA, www.graphpad.com. Data were assessed for normality using a Shapiro-Wilk test in SigmaPlot 14, and the homogeneity of variances was verified. One-way analysis of variance, followed by Duncan's post hoc test, was conducted to identify statistically significant (two-sided) differences between nanoplastic and nanoplastic-BC treatments. To determine significant differences between PS and PVC, a t-test was applied. Average Log2(FCs) were calculated for both nanoplastics at all time points, and significantly enriched or depleted proteins were determined using a Student's t-test with subsequent p-value adjustment according to Benjamini & Hochberg (Additional file proteome: Table 1). The correlation of the protein containing modules in the WGCNA model with the two nanoplastics at the four time points or the combination of all time points was determined using Pearson correlation and Student asymptotic p-values. Data from the qPCR and viability tests are presented as mean and standard dviation, while for the permeability tests, data are presented as mean and standard error of the mean .

Funding

This work received financial support from the UEF Water research program, which is jointly funded by the Saastamoinen Foundation, the Wihuri Foundation and the Olvi Foundation. IL acknowledges the EU-funded CompSafeNano project (Grant Agreement nº 101008099). KS is grateful for funding by the German Research Foundation (project number 530364326). The School of Pharmacy mass spectrometry laboratory is supported by Biocenter Finland and Biocenter Kuopio.

Author statement

F.A.M. designed the experiments, conceptualized, supervised, wrote, and reviewed the study. F.A.M., I.L., J.K., and M.B. performed the protein plasma incubation. F.A.M. and J.K., designed nanoplastics. S.L., F.A.M., M.B., S. P., and J. N., performed the cell exposure experiment. F.A.M., J.L., A.K., S.B., and A.Z., performed the nanoplastic characterization and quantification. I.K., F.A.M, S.A., K.S., M.v.B., I.L., Z.G., and C.C., studied the biotransformation of particles in different physiological media and performed mass spectrometry as well as data analysis. All co-authors contributed to designing the experiment, writing, and editing the paper.

CRediT authorship contribution statement

Martin von Bergen: Supervision, Resources, Investigation, Funding acquisition, Conceptualization. **Fazel Abdolahpur Monikh:** Writing – original draft, Supervision, Methodology, Investigation, Funding acquisition, Formal analysis, Data curation, Conceptualization. **Jonna Niskanen:** Writing – review & editing, Software, Methodology. **Mandar Bandekar:** Writing – review & editing, Methodology, Investigation. **Iseult Lynch:** Writing – review & editing, Validation, Supervision, Data curation, Conceptualization. **Alessandra Zanut:** Writing – review & editing, Software, Investigation, Formal analysis. **Sanni Peltonen:** Writing – original draft, Validation, Methodology, Formal analysis, Data curation. **Jussi V.K. Kukkonen:** Supervision, Funding acquisition, Conceptualization. **Seppo Auriola:** Writing – review & editing, Software, Methodology, Data curation. **Chunying Chen:** Supervision, Investigation, Conceptualization. **Kristin Schubert:** Supervision, Methodology, Formal analysis. **Sara Bogialli:** Supervision, Resources, Investigation, Conceptualization. **Jukka Kekäläinen:** Investigation, Formal analysis. **Zhiling Guo:** Writing – review & editing, Formal analysis, Data curation. **Isabel Karkossa:** Writing – original draft, Software, Methodology, Formal analysis, Data curation. **Jari T.T. Leskinen:** Writing – review & editing, Visualization, Software, Investigation, Data curation. **Arto Koistinen:** Supervision, Resources, Funding acquisition. **Šárka Lehtonen:** Writing – review & editing, Methodology, Funding acquisition, Formal analysis, Data curation.

Declaration of Competing Interest

The authors declare that they have no known competing financial interests or personal relationships that could have appeared to influence the work reported in this paper.

Data availability

The data will be shared

Acknowledgments

The authors would like to take this opportunity to thank their institutions and especially the UFZ-funded ProMetheus platform for proteomics and metabolomics for the support of this project. In addition, the authors want to thank Maj Schuster for excellent technical assistance. We also thank Virpi Miettinen for helping with sample preparation for SEM and TEM and Dr. Emilia Uurasjärvi for help in determining the SMPs chemical composition using Raman Spectroscopy. We would also like to thank Pasi Yli-Pirilä for his help in performing the ICP-MS measurements. We are grateful to SIB Labs Kuopio Electron Microscopy Facility, part of Biocenter Kuopio and Biocenter Finland for technical and financial assistance.

Appendix A. Supporting information

Supplementary data associated with this article can be found in the online version at doi:10.1016/j.nantod.2024.102466.

References

[1] A.L. Andrady, Microplastics in the marine environment, Mar. Pollut. Bull. 62 (2011) 1596–1605, https://doi.org/10.1016/j.marpolbul.2011.05.030.
[2] H.Y. Sintim, A.I. Bary, D.G. Hayes, M.E. English, S.M. Schaeffer, C.A. Miles, A. Zelenyuk, K. Suski, M. Flury, Release of micro- and nanoparticles from

biodegradable plastic during in situ composting, Sci. Total Environ. 675 (2019) 686–693, https://doi.org/10.1016/j.scitotenv.2019.04.179.
[3] F. Abdolahpur Monikh, S.F. Hansen, M.G. Vijver, E. Kentin, M.B. Nielsen, A. Baun, K. Syberg, I. Lynch, E. Valsami-Jones, W.J.G.M. Peijnenburg, Can current regulations account for intentionally produced nanoplastics? Environ. Sci. Technol. 56 (2022) 3836–3839, https://doi.org/10.1021/acs.est.2c00965.
[4] A. van Wezel, I. Caris, S.A.E. Kools, Release of primary microplastics from consumer products to wastewater in the Netherlands, Environ. Toxicol. Chem. 35 (2016) 1627–1631, https://doi.org/10.1002/etc.3316.
[5] L.M. Hernandez, E.G. Xu, H.C.E. Larsson, R. Tahara, V.B. Maisuria, N. Tufenkji, Plastic teabags release billions of microparticles and nanoparticles into tea, Environ. Sci. Technol. 53 (2019) 12300–12310, https://doi.org/10.1021/acs.est.9b02540.
[6] A.D. Vethaak, J. Legler, Microplastics and human health, Science 371 (2021) 672–674, https://doi.org/10.1126/science.abe5041.
[7] A. Sun, W.-X. Wang, Human exposure to microplastics and its associated health risks, Environ. Health 1 (2023) 139–149, https://doi.org/10.1021/envhealth.3c00053.
[8] C. Yong, S. Valiyaveettil, B. Tang, Toxicity of microplastics and nanoplastics in mammalian systems, Int. J. Environ. Res. Public Health 17 (2020) 1509, https://doi.org/10.3390/ijerph17051509.
[9] R. Martin-Folgar, C. Sabroso, A.I. Cañas-Portilla, M. Torres-Ruíz, M.C. González-Caballero, H. Dorado, I. Velasco, M. Morales, DNA damage and molecular level effects induced by polystyrene (PS) nanoplastics (NPs) after Chironomus riparius (Diptera) larvae, Chemosphere 346 (2024), https://doi.org/10.1016/j.chemosphere.2023.140552.
[10] K.E. Wheeler, A.J. Chetwynd, K.M. Fahy, B.S. Hong, J.A. Tochihuitl, L.A. Foster, I. Lynch, Environmental dimensions of the protein corona, Nat. Nanotechnol. 16 (2021) 617–629, https://doi.org/10.1038/s41565-021-00924-1.
[11] J. La Nasa, T. Lomonaco, E. Manco, A. Ceccarini, R. Fuoco, A. Corti, F. Modugno, V. Castelvetro, I. Degano, Plastic breeze: volatile organic compounds (VOCs) emitted by degrading macro- and microplastics analyzed by selected ion flow-tube mass spectrometry, Chemosphere 270 (2021), https://doi.org/10.1016/j.chemosphere.2020.128612.
[12] A. Vismara, A. Gautieri, Molecular insights into nanoplastics-peptides binding and their interactions with the lipid membrane, Biophys. Chem. 308 (2024), https://doi.org/10.1016/j.bpc.2024.107213.
[13] M. Mahmoudi, I. Lynch, M.R. Ejtehadi, M.P. Monopoli, F.B. Bombelli, S. Laurent, Protein−nanoparticle interactions: opportunities and challenges, Chem. Rev. 111 (2011) 5610–5637, https://doi.org/10.1021/cr100440g.
[14] E. Hellstrand, I. Lynch, A. Andersson, T. Drakenberg, B. Dahlbäck, K.A. Dawson, S. Linse, T. Cedervall, Complete high-density lipoproteins in nanoparticle corona, FEBS J. 276 (2009) 3372–3381, https://doi.org/10.1111/j.1742-4658.2009.07062.x.
[15] K.K. Nanda, A. Maisels, F.E. Kruis, H. Fissan, S. Stappert, Higher Surface energy of free nanoparticles, Phys. Rev. Lett. 91 (2003) 106102, https://doi.org/10.1103/PhysRevLett.91.106102.
[16] Y. Tan, X. Zhu, D. Wu, E. Song, Y. Song, Compromised autophagic effect of polystyrene nanoplastics mediated by protein corona was recovered after lysosomal degradation of corona, Environ. Sci. Technol. 54 (2020) 11485–11493, https://doi.org/10.1021/acs.est.0c04097.
[17] P.M. Gopinath, V. Saranya, S. Vijayakumar, M. Mythili Meera, S. Ruprekha, R. Kunal, A. Pranay, J. Thomas, A. Mukherjee, N. Chandrasekaran, Assessment on interactive prospectives of nanoplastics with plasma proteins and the toxicological impacts of virgin, coronated and environmentally released-nanoplastics, Sci. Rep. 9 (2019) 8860, https://doi.org/10.1038/s41598-019-45139-6.
[18] Z. Zhang, X. Dong, W. Wan, H. Guo, R. Sun, H. Feng, M. Wang, Z. Wang, H. Jin, J. Sun, Q. Xia, Q. Zhao, D. Shen, Z. Gao, Y. Liu, Unraveling intracellular protein corona components of nanoplastics via photocatalytic protein proximity labeling, Anal. Chem. 96 (2024) 4978–4986, https://doi.org/10.1021/acs.analchem.4c00050.
[19] F. Abdolahpur Monikh, S. Holm, R. Kortet, M. Bandekar, J. Kekäläinen, A. Koistinen, J.T.T. Leskinen, J. Akkanen, H. Huuskonen, A. Valtonen, L. Dupuis, W. Peijnenburg, I. Lynch, E. Valsami-Jones, J.V.K. Kukkonen, Quantifying the trophic transfer of sub-micron plastics in an assembled food chain, Nano Today 46 (2022) 101611, https://doi.org/10.1016/j.nantod.2022.101611.
[20] F. Bertoli, D. Garry, M.P. Monopoli, A. Salvati, K.A. Dawson, The intracellular destiny of the protein corona: a study on its cellular internalization and evolution, ACS Nano 10 (2016) 10471–10479, https://doi.org/10.1021/acsnano.6b06411.
[21] R. Madathiparambil Visalakshan, L.E. González García, M.R. Benzigar, A. Ghazaryan, J. Simon, A. Mierczynska-Vasilev, T.D. Michl, A. Vinu, V. Mailänder, S. Morsbach, K. Landfester, K. Vasilev, The influence of nanoparticle shape on protein corona formation, Small 16 (2020) e2000285, https://doi.org/10.1002/smll.202000285.
[22] M. Lundqvist, J. Stigler, G. Elia, I. Lynch, T. Cedervall, K.A. Dawson, Nanoparticle size and surface properties determine the protein corona with possible implications for biological impacts, Proc. Natl. Acad. Sci. USA 105 (2008) 14265–14270, https://doi.org/10.1073/pnas.0805135105.
[23] I. Lynch, K.A. Dawson, Protein-nanoparticle interactions, Nano Today 3 (2008) 40–47, https://doi.org/10.1016/S1748-0132(08)70014-8.
[24] M. Lundqvist, J. Stigler, T. Cedervall, T. Berggård, M.B. Flanagan, I. Lynch, G. Elia, K. Dawson, The evolution of the protein corona around nanoparticles: a test study, ACS Nano (2011), https://doi.org/10.1021/nn202458g.
[25] A.J. Chetwynd, I. Lynch, The rise of the nanomaterial metabolite corona, and emergence of the complete corona, Environ. Sci. Nano 7 (2020) 1041–1060, https://doi.org/10.1039/c9en00938h.
[26] D. Walczyk, F.B. Bombelli, M.P. Monopoli, I. Lynch, K.A. Dawson, What the cell "sees" in bionanoscience, J. Am. Chem. Soc. 132 (2010) 5761–5768, https://doi.org/10.1021/ja910675v.
[27] B.V. Zlokovic, The blood-brain barrier in health and chronic neurodegenerative disorders, Neuron 57 (2008) 178–201, https://doi.org/10.1016/j.neuron.2008.01.003.
[28] Z. Guo, P. Zhang, S. Chakraborty, A.J. Chetwynd, F. Abdolahpur Monikh, C. Stark, H. Ali-Boucetta, S. Wilson, I. Lynch, E. Valsami-Jones, Biotransformation modulates the penetration of metallic nanomaterials across an artificial blood-brain barrier model, Proc. Natl. Acad. Sci. USA 118 (2021) 1–10, https://doi.org/10.1073/pnas.2105245118.
[29] Z. Guo, P. Zhang, Y. Luo, H.Q. Xie, S. Chakraborty, F.A. Monikh, L. Bu, Y. Liu, Y. Ma, Z. Zhang, E. Valsami-Jones, B. Zhao, I. Lynch, Intranasal exposure to ZnO nanoparticles induces alterations in cholinergic neurotransmission in rat brain, Nano Today 35 (2020) 100977, https://doi.org/10.1016/j.nantod.2020.100977.
[30] F. Abdolahpur Monikh, Z. Guo, P. Zhang, M.G. Vijver, I. Lynch, E. Valsami-Jones, W.J.G.M. Peijnenburg, An analytical workflow for dynamic characterization and quantification of metal-bearing nanomaterials in biological matrices, Nat. Protoc. 17 (2022) 1926–1952, https://doi.org/10.1038/s41596-022-00701-x.
[31] I. Zanoni, J.G. Keller, U.G. Sauer, P. Müller, L. Ma-Hock, K.A. Jensen, A.L. Costa, W. Wohlleben, Dissolution rate of nanomaterials determined by ions and particle size under lysosomal conditions: contributions to standardization of simulant fluids and analytical methods, Chem. Res. Toxicol. 35 (2022) 963–980, https://doi.org/10.1021/acs.chemrestox.1c00418.
[32] I. Zanoni, J.G. Keller, U.G. Sauer, P. Müller, L. Ma-Hock, K.A. Jensen, A.L. Costa, W. Wohlleben, Dissolution rate of nanomaterials determined by ions and particle size under lysosomal conditions: contributions to standardization of simulant fluids and analytical methods, Chem. Res. Toxicol. 35 (2022) 963–980, https://doi.org/10.1021/acs.chemrestox.1c00418.
[33] V. Kopatz, K. Wen, T. Kovács, A.S. Keimowitz, V. Pichler, J. Widder, A.D. Vethaak, O. Hollóczki, L. Kenner, Micro- and nanoplastics breach the blood–brain barrier (BBB): biomolecular corona's role revealed, Nanomaterials 13 (2023), https://doi.org/10.3390/nano13081404.
[34] S. Shan, Y. Zhang, H. Zhao, T. Zeng, X. Zhao, Polystyrene nanoplastics penetrate across the blood-brain barrier and induce activation of microglia in the brain of mice, Chemosphere 298 (2022) 134261, https://doi.org/10.1016/j.chemosphere.2022.134261.
[35] X. Zhao, J. Sun, L. Zhou, M. Teng, L. Zhao, Y. Li, F. Wu, Defining the size ranges of polystyrene nanoplastics according to their ability to cross biological barriers, Environ. Sci. Nano 10 (2023) 2634–2645, https://doi.org/10.1039/D3EN00491K.
[36] F. Abdolahpur Monikh, M.G. Vijver, D.M. Mitrano, H.A. Leslie, Z. Guo, P. Zhang, I. Lynch, E. Valsami-Jones, W.J.G.M. Peijnenburg, The analytical quest for sub-micron plastics in biological matrices, Nano Today 41 (2021) 101296, https://doi.org/10.1016/j.nantod.2021.101296.
[37] F. Abdolahpur Monikh, A. Baun, N.B. Hartmann, R. Kortet, J. Akkanen, J.S. Lee, H. Shi, E. Lahive, E. Uurasjärvi, N. Tufenkji, K. Altmann, Y. Wiesner, H.P. Grossart, W. Peijnenburg, J.V.K. Kukkonen, Exposure protocol for ecotoxicity testing of microplastics and nanoplastics, Nat. Protoc. 18 (2023) 3534–3564, https://doi.org/10.1038/s41596-023-00886-9.
[38] L. Marigliano, B. Grassl, J. Szpunar, S. Reynaud, J. Jiménez-Lamana, Nanoplastic labelling with metal probes: analytical strategies for their sensitive detection and quantification by ICP mass spectrometry, Molecules 26 (2021) 7093, https://doi.org/10.3390/molecules26237093.
[39] M. Bandekar, F. Abdolahpur Monikh, J. Kekäläinen, T. Tahvanainen, R. Kortet, P. Zhang, Z. Guo, J. Akkanen, J.T.T. Leskinen, M.A. Gomez-Gonzalez, G. Krishna Darbha, H.P. Grossart, E. Valsami-Jones, J.V.K. Kukkonen, Submicron plastic adsorption by peat, accumulation in sphagnum mosses and influence on bacterial communities in peatland ecosystems, Environ. Sci. Technol. 56 (2022) 15661–15671, https://doi.org/10.1021/acs.est.2c04892.
[40] F. Abdolahpur Monikh, L. Chupani, M.G. Vijver, W.J.G.M. Peijnenburg, Parental and trophic transfer of nanoscale plastic debris in an assembled aquatic food chain as a function of particle size, Environ. Pollut. 269 (2021) 116066, https://doi.org/10.1016/j.envpol.2020.116066.
[41] F. Abdolahpur Monikh, L. Chupani, M.G. Vijver, M. Vancová, W.J.G. M. Peijnenburg, Analytical approaches for characterizing and quantifying engineered nanoparticles in biological matrices from an (eco)toxicological perspective: old challenges, new methods and techniques, Sci. Total Environ. 660 (2019) 1283–1293, https://doi.org/10.1016/j.scitotenv.2019.01.105.
[42] D.J. Pochapski, C. Carvalho Dos Santos, G.W. Leite, S.H. Pulcinelli, C.V. Santilli, Zeta potential and colloidal stability predictions for inorganic nanoparticle dispersions: effects of experimental conditions and electrokinetic models on the interpretation of results, Langmuir 37 (2021) 13379–13389, https://doi.org/10.1021/acs.langmuir.1c02056.
[43] M. Riediker, D. Zink, W. Kreyling, G. Oberdörster, A. Elder, U. Graham, I. Lynch, A. Duschl, G. Ichihara, S. Ichihara, T. Kobayashi, N. Hisanaga, M. Umezawa, T.-J. Cheng, R. Handy, M. Gulumian, S. Tinkle, F. Cassee, Particle toxicology and health - where are we? Part. Fibre Toxicol. 16 (2019) 19, https://doi.org/10.1186/s12989-019-0302-8.
[44] F.M. Cavagna, F. Maggioni, P.M. Castelli, M. Daprà, L.G. Imperatori, V. Lorusso, B. G. Jenkins, Gadolinium chelates with weak binding to serum proteins: A new class of high-efficiency, general purpose contrast agents for magnetic resonance imaging, Investig. Radiol. 32 (1997) 780–796, https://doi.org/10.1097/00004424-199712000-00009.
[45] T. Cedervall, I. Lynch, S. Lindman, T. Berggard, E. Thulin, H. Nilsson, K.A. Dawson, S. Linse, Understanding the nanoparticle-protein corona using methods to quantify

exchange rates and affinities of proteins for nanoparticles, Proc. Natl. Acad. Sci. USA 104 (2007) 2050–2055, https://doi.org/10.1073/pnas.0608582104.
[46] M.P. Monopoli, C. Åberg, A. Salvati, K.A. Dawson, Biomolecular coronas provide the biological identity of nanosized materials, Nat. Nanotechnol. 7 (2012) 779–786, https://doi.org/10.1038/nnano.2012.207.
[47] S. Kihara, N.J. Van Der Heijden, C.K. Seal, J.P. Mata, A.E. Whitten, I. Köper, D. J. McGillivray, Soft and hard interactions between polystyrene nanoplastics and human serum albumin protein corona, Bioconjug. Chem. 30 (2019) 1067–1076, https://doi.org/10.1021/acs.bioconjchem.9b00015.
[48] F. Abdolahpur Monikh, M.G. Vijver, R. Kortet, I. Lynch, W.J.G.M. Peijnenburg, Emerging investigator series: perspectives on toxicokinetics of nanoscale plastic debris in organisms, Environ. Sci. Nano 9 (2022) 1566–1577, https://doi.org/10.1039/D1EN00425E.
[49] V. Stone, S. Gottardo, E.A.J. Bleeker, H. Braakhuis, S. Dekkers, T. Fernandes, A. Haase, N. Hunt, D. Hristozov, P. Jantunen, N. Jeliazkova, H. Johnston, L. Lamon, F. Murphy, K. Rasmussen, H. Rauscher, A.S. Jiménez, C. Svendsen, D. Spurgeon, S. Vázquez-Campos, W. Wohlleben, A.G. Oomen, A framework for grouping and read-across of nanomaterials- supporting innovation and risk assessment, Nano Today 35 (2020) 100941, https://doi.org/10.1016/j.nantod.2020.100941.
[50] F. Abdolahpur Monikh, L. Chupani, I. Karkossa, Z. Gardian, D. Arenas-Lago, M. von Bergen, K. Schubert, V. Piackova, E. Zuskova, W. Jiskoot, M.G. Vijver, W.J.G. M. Peijnenburg, An environmental ecocorona influences the formation and evolution of the biological corona on the surface of single-walled carbon nanotubes, NanoImpact 22 (2021) 100315, https://doi.org/10.1016/j.impact.2021.100315.
[51] S. Tenzer, D. Docter, S. Rosfa, A. Wlodarski, J. Kuharev, A. Rekik, S.K. Knauer, C. Bantz, T. Nawroth, C. Bier, J. Sirirattanapan, W. Mann, L. Treuel, R. Zellner, M. Maskos, H. Schild, R.H. Stauber, Nanoparticle size is a critical physicochemical determinant of the human blood plasma corona: a comprehensive quantitative proteomic analysis, ACS Nano 5 (2011) 7155–7167, https://doi.org/10.1021/nn201950e.
[52] S. Ritz, S. Schöttler, N. Kotman, G. Baier, A. Musyanovych, J. Kuharev, K. Landfester, H. Schild, O. Jahn, S. Tenzer, V. Mailänder, Protein corona of nanoparticles: distinct proteins regulate the cellular uptake, Biomacromolecules 16 (2015) 1311–1321, https://doi.org/10.1021/acs.biomac.5b00108.
[53] C.D. Walkey, W.C.W. Chan, Understanding and controlling the interaction of nanomaterials with proteins in a physiological environment, Chem. Soc. Rev. 41 (2012) 2780–2799, https://doi.org/10.1039/c1cs15233e.
[54] D. Ye, K.A. Dawson, I. Lynch, A TEM protocol for quality assurance of in vitro cellular barrier models and its application to the assessment of nanoparticle transport mechanisms across barriers, Analyst 140 (2015) 83–97, https://doi.org/10.1039/C4AN01276C.
[55] R. Lenz, K. Enders, T.G. Nielsen, Microplastic exposure studies should be environmentally realistic, Proc. Natl. Acad. Sci. USA 113 (2016) E4121–E4122, https://doi.org/10.1073/pnas.1606615113.
[56] G. Tosi, R.A. Fano, L. Bondioli, L. Badiali, R. Benassi, F. Rivasi, B. Ruozi, F. Forni, M.A. Vandelli, Investigation on mechanisms of glycopeptide nanoparticles for drug delivery across the blood-brain barrier, Nanomedicine 6 (2011) 423–436, https://doi.org/10.2217/nnm.11.11.
[57] A.N. Vijayan, J. Indrakumar, S. Gomathinayagam, K.M. Gothandam, P. S. Korrapati, Bi-functional aspects of peptide decorated plga nanocarriers for enhanced translocation across the blood-brain barrier through macropinocytosis, Macromol. Res. 30 (2022) 557–570, https://doi.org/10.1007/s13233-022-0061-5.
[58] A. Sahin, D. Yoyen-Ermis, S. Caban-Toktas, U. Horzum, Y. Aktas, P. Couvreur, G. Esendagli, Y. Capan, Evaluation of brain-targeted chitosan nanoparticles through blood–brain barrier cerebral microvessel endothelial cells, J. Microencapsul. 34 (2017) 659–666, https://doi.org/10.1080/02652048.2017.1375039.
[59] X.H. Li, Y.Z. Meng, Q. Zhu, S.C. Tjong, Thermal decomposition characteristics of poly(propylene carbonate) using TG/IR and Py-GC/MS techniques, Polym. Degrad. Stab. 81 (2003) 157–165, https://doi.org/10.1016/S0141-3910(03)00085-5.
[60] F. Abdolahpur Monikh, L. Chupani, D. Arenas-Lago, Z. Guo, P. Zhang, G.K. Darbha, E. Valsami-Jones, I. Lynch, M.G. Vijver, P.M. van Bodegom, W.J.G.M. Peijnenburg, Particle number-based trophic transfer of gold nanomaterials in an aquatic food chain, Nat. Commun. 12 (2021) 899, https://doi.org/10.1038/s41467-021-21164-w.
[61] M. Riediker, D. Zink, W. Kreyling, G. Oberdörster, A. Elder, U. Graham, I. Lynch, A. Duschl, G. Ichihara, S. Ichihara, T. Kobayashi, N. Hisanaga, M. Umezawa, T.-J. Cheng, R. Handy, M. Gulumian, S. Tinkle, F. Cassee, Correction to: particle toxicology and health - where are we? Part. Fibre Toxicol. 16 (2019) 26, https://doi.org/10.1186/s12989-019-0308-2.
[62] D. Walczyk, F.B. Bombelli, M.P. Monopoli, I. Lynch, K.A. Dawson, What the cell "sees" in bionanoscience, J. Am. Chem. Soc. 132 (2010) 5761–5768, https://doi.org/10.1021/ja910675v.
[63] A. Lesniak, F. Fenaroli, M.P. Monopoli, C. Åberg, K.A. Dawson, A. Salvati, Effects of the presence or absence of a protein corona on silica nanoparticle uptake and impact on cells, ACS Nano 6 (2012) 5845–5857, https://doi.org/10.1021/nn300223w.
[64] M.C. Heinrich, M.K. Kuhlmann, S. Kohlbacher, M. Scheer, A. Grgic, M. B. Heckmann, M. Uder, Cytotoxicity of iodinated and gadolinium-based contrast agents in renal tubular cells at angiographic concentrations: in vitro study, Radiology 242 (2007) 425–434, https://doi.org/10.1148/radiol.2422060245.
[65] S. Noerman, M. Kokla, V.M. Koistinen, M. Lehtonen, T.P. Tuomainen, C. Brunius, J. K. Virtanen, K. Hanhineva, Associations of the serum metabolite profile with a healthy Nordic diet and risk of coronary artery disease, Clin. Nutr. 40 (2021) 3250–3262, https://doi.org/10.1016/j.clnu.2020.10.051.
[66] Z. Wang, I. Karkossa, H. Großkopf, U. Rolle-Kampczyk, J. Hackermüller, M. von Bergen, K. Schubert, Comparison of quantitation methods in proteomics to define relevant toxicological information on AhR activation of HepG2 cells by BaP, Toxicology 448 (2021) 152652, https://doi.org/10.1016/j.tox.2020.152652.
[67] P. Langfelder, S. Horvath, WGCNA: an R package for weighted correlation network analysis, BMC Bioinforma. 9 (2008), https://doi.org/10.1186/1471-2105-9-559.
[68] I. Karkossa, A. Bannuscher, B. Hellack, A. Bahl, S. Buhs, P. Nollau, A. Luch, K. Schubert, M. Von Bergen, A. Haase, An in-depth multi-omics analysis in RLE-6TN rat alveolar epithelial cells allows for nanomaterial categorization, Part. Fibre Toxicol. 16 (2019), https://doi.org/10.1186/s12989-019-0321-5.
[69] A. Harding, E. Cortez-Toledo, N.L. Magner, J.R. Beegle, D.P. Coleal-Bergum, D. Hao, A. Wang, J.A. Nolta, P. Zhou, Highly efficient differentiation of endothelial cells from pluripotent stem cells requires the MAPK and the PI3K pathways, Stem Cells 35 (2017) 909–919, https://doi.org/10.1002/stem.2577.
[70] R. Krencik, S.C. Zhang, Directed differentiation of functional astroglial subtypes from human pluripotent stem cells, Nat. Protoc. 6 (2011) 1710–1717, https://doi.org/10.1038/nprot.2011.405.
[71] M. Oksanen, A.J. Petersen, N. Naumenko, K. Puttonen, Š. Lehtonen, M. Gubert Olivé, A. Shakirzyanova, S. Leskelä, T. Sarajärvi, M. Viitanen, J.O. Rinne, M. Hiltunen, A. Haapasalo, R. Giniatullin, P. Tavi, S.C. Zhang, K.M. Kanninen, R. H. Hämäläinen, J. Koistinaho, PSEN1 Mutant iPSC-derived model reveals severe astrocyte pathology in alzheimer's disease, Stem Cell Rep. 9 (2017) 1885–1897, https://doi.org/10.1016/j.stemcr.2017.10.016.
[72] M.J. Stebbins, H.K. Wilson, S.G. Canfield, T. Qian, S.P. Palecek, E.V. Shusta, Differentiation and characterization of human pluripotent stem cell-derived brain microvascular endothelial cells, Methods 101 (2016) 93–102, https://doi.org/10.1016/j.ymeth.2015.10.016.